Gravitational wave echoes from strange quark stars in the equation of state with density-dependent quark masses*

Jian-Feng Xu ,[1,†] Lei Cui,[1] Zhen-Yan Lu ,[2,‡] Cheng-Jun Xia,[3,§] and Guang-Xiong Peng[4,5,¶]

[1]*School of arts and sciences, Suqian University, Suqian 223800, China*
[2]*Hunan Provincial Key Laboratory of Intelligent Sensors and Advanced Sensor Materials, School of Physics and Electronics, Hunan University of Science and Technology, Xiangtan 411201, China*
[3]*Center for Gravitation and Cosmology, College of Physical Science and Technology, Yangzhou University, Yangzhou 225009, China*
[4]*School of Nuclear Science and Technology, University of Chinese Academy of Sciences, Beijing 100049, China*
[5]*Institute of High Energy Physics, Chinese Academy of Sciences, Beijing 100049, China*

According to the recent studies, the gravitational wave (GW) echoes are expected to be generated by quark stars composed of ultrastiff quark matter. The ultrastiff equations of state (EOS) for quark matter were usually obtained either by a simple bag model with artificially assigned sound velocity or by employing interacting strange quark matter (SQM) depicted by simple reparameterization and rescaling. In this study, we investigate GW echoes with EOSs for SQM in the framework of the equivparticle model with density-dependent quark masses and pairing effects. We conclude that strange quark stars (SQSs) can be sufficiently compact to possess a photon sphere capable of generating GW echoes with frequencies in the range of approximately 20 kHz. However, SQSs cannot account for the observed 72 Hz signal in GW170817 event. Furthermore, we determined that quark-pairing effects play a crucial role in enabling SQSs to satisfy the necessary conditions for producing these types of echoes.

Keywords: Strange quark star, Gravitational wave echoes, Color-flavour-locked phase, Strange quark matter

I. INTRODUCTION

The detection of gravitational waves (GWs) by the LIGO and Virgo collaborations [1–5] has significant implications in astrophysics, opening up new avenues for research on black holes, neutron stars, and other dense stellar objects [6, 7]. It was suggested that GW echoes [8–10] were expected as a generic feature of quantum corrections at the horizon scale in the postmerger GW signals from binary coalescence events, particularly those involving black holes. In general, the emission of GW echoes requires dense stellar objects featuring a photon sphere located at $R_{\rm p} = 3M$, where M denotes the mass of the dense object [11–14]. The photon sphere can partially trap the GW to produce the GW echoes.

This type of a photon sphere can be found both in black holes [15] and superdense stars [16, 17], whose radii should be smaller than $R_{\rm p}$. For black holes, besides the photon sphere, the GW echoes necessitate a secondary reflecting surface to circumvent GW absorption, which may be related to quantum effects in proximity to the black hole horizon [18]. The possible occurrence of GW echoes at a frequency of approximately 72 Hz, with a statistical significance level of 4.2σ, was first investigated in Ref. [19] for the GW170817 event, where the GW echoes were interpreted as a result of quantum effects close to the black hole horizon.

However, Ref. [20] indicated that GW echoes can be generated not only by quantum corrections at the horizon scale but also by exotic super-compact objects [21, 22]. Moreover, a simplified incompressible equation of state was utilized, revealing that a highly compact stellar object with radius close to the Buchdahl's radius [23] $R_{\rm B} = 9/4M$ is required to produce GW echoes with such low frequencies. Specifically, the Buchdahl's radius is the minimum radius for compact stars [23]. Additionally, in order for compact stars to produce GW echoes, the radii of compact stars must fall within the range of $R_{\rm B} < R < R_{\rm P}$. This compactness criterion essentially precludes the realistic equation of states (EOSs) for neutron stars [20]. Consequently, researchers are exploring alternative compact stellar objects, such as strange quark stars (SQSs) [24], which consist of strange quark matter (SQM) [25–28].

In Ref. [29], the authors verified whether a more realistic EOS of quark stars can emit GW echoes. They employed the confined-isospin-density-dependent-mass model with additional scalar and vector Coulomb terms of SQM [30] and confirmed that SQSs with realistic EOS cannot be categorized as ultra-compact objects to feature a photon sphere to generate GW echoes. Moreover, in Ref. [31], the authors utilized an interacting quark matter EOS unifying interacting phases via a simple reparameterization and rescaling. They found that GW echoes are possible for QSs with large center pressure. Furthermore, GW echoes were examined in $f(R,T)$ gravity metric formalism within MIT bag model and the color-flavor-locked (CFL) EOSs. The authors indicated that, under some considerations, the realistic interacting QM can lead to stellar structures, which are sufficiently compact to feature a photon sphere outside the stellar boundary, and thereby, can echo GWs [32, 33]. Additionally, the author

* This work was supported by the National Natural Science Foundation of China (Nos. 12005005, 12205093, 12275234, and 11875052), the National SKA Program of China (No. 2020SKA0120300), the Hunan Provincial Nature Science Foundation of China (No. 2021JJ40188), the Scientific Research Start-up Fund of Talent Introduction of Suqian University (No. Xiao2022XRC061), Suqian Key Laboratory of High Performance Composite Materials (M202109), and Suqian University Multi functional Material R&D Platform (2021pt04).
† xujf@squ.edu.cn
‡ luzhenyan@hnust.edu.cn
§ cjxia@yzu.edu.cn
¶ gxpeng@ucas.ac.cn

investigated the GW echoes from SQSs for various EOSs, including MIT bag model and linear and polytropic EOSs. However, only the MIT bag model and linear polytropic EOSs were found to emit GW echoes at a frequency range of approximately tens of kilohertz [34]. In a recent study [35], the GW echoes produced by strangeon stars composed of strange-cluster matter, which is in the solid state, were investigated. The authors recasted the EOS of strange-cluster matter into dimensionless forms via reparameterization and rescaling. Furthermore, they concluded that strangeon stars are typically compact enough to have a photon sphere. This sphere reflects the GWs that fall within the gravitational potential barrier, producing GW echoes with a minimum echo frequency of approxiamtely 8 kHz, extending even to frequencies as low as $\mathcal{O}(100)$ Hertz.

Nonetheless, in the aforementioned studies, the investigations concerning GW echoes have primarily concentrated on either a basic MIT bag model or parameterized EOSs for SQM. In this study, we employ EOSs for SQM based on the equivparticle model with density-dependent quark masses. Within this model, quark masses are scaled according to the baryon number density, replicating the complex interactions among quarks [36].

This model was initially developed as a quark mass-density-dependent model [37–40], and later renamed as the equivparticle model after explicitly introducing the concept of effective quark chemical potential [41]. Given its clear physical picture and accurate thermodynamic treatments, the model has been widely utilized in the study of quark matter properties and structures of quark stars [42–46]. In Ref. [47], we investigated the symmetry energy of SQM and tidal deformability of SQSs within this model. Our findings indicate that the region of absolute stability for SQM can be significantly widened with sufficiently large isospin symmetric parameter, yielding results that simultaneously satisfy the constraints imposed by astrophysical observations of PSR J1614-2230, with 1.928 ± 0.017 $M_\odot$ [48] and tidal deformability $70 \leq \Lambda_{1.4} \leq 580$ measured in the GW170817 event [7]. On application of the EOSs in this model, we determine that SQSs can produce GW echoes with the frequencies in the order of kilohertz, which is consistent with previous findings, provided that they are composed of SQM in the CFL phase [32, 33].

The paper is organized as follows: Section II provides a brief overview of the EOSs for SQM in CFL phase within the equivparticle model. Section III presents the process of calculating the GW echoes and scrutinizes the corresponding numerical results. Finally, a concise summary is presented in Sect. IV.

II. EOS OF CFL QUARK MATTER IN EQUIVPARTICLE MODEL

The thermodynamic potential density for CFL SQM can be expressed as:

$$\begin{aligned}\Omega_{\rm CFL} &= -\sum_{i=\rm u,d,s}\frac{g_i}{2\pi^2}\int_0^{\nu}\left(\mu_i-\sqrt{p^2+m_i^2}\right)p^2\,{\rm d}p\\ &\quad -\frac{3\Delta^2\bar{\mu}^2}{\pi^2}+B,\end{aligned} \tag{1}$$

where $g_i = 2\times 3 = 6$ corresponds to degenerate factor, ν denotes the common Fermi momentum, $\bar{\mu} \equiv (\mu_{\rm u}+\mu_{\rm d}+\mu_{\rm s})/3$ is the averaged chemical potential of quarks, Δ denotes the quark pair energy gap, B denotes the bag constant, which can be expressed as $B^{1/4} = 180$ MeV in the following calculation, and m_i denotes density-dependent quark mass which can be scaled as:

$$m_i = m_{i0} + m_{\rm I} = m_{i0} + \frac{D}{n_b^{1/3}}, \tag{2}$$

where $m_{\rm u0} = m_{\rm d0} = 5$ MeV and $m_{\rm s0} = 100$ MeV are the quark current masses [49], $m_{\rm I}$ denotes the interacting part and is the same for all flavors, and D denotes a model parameter representing the strength of confinement. Due to the lack of accurate value of Δ, in this model Δ is considered to be a free model parameter. It should be emphasized that the quark chemical potential μ_i is effective. Furthermore, the real chemical potential $\mu_{i,\rm real}$ can be related to the effective one due to the density-dependent quark mass [41]. To ensure maximum paring, the common Fermi momentum ν can be obtained by taking the derivative of $\Omega_{\rm CFL}$ with respect to ν, i.e., $\partial\Omega_{\rm CFL}/\partial\nu = 0$, yielding

$$\sum_i \sqrt{\nu^2+m_i^2} = 3\bar{\mu}. \tag{3}$$

The integration in Eq. (1) can be conducted as follows:

$$\begin{aligned}&\Omega_{\rm CFL} =\\ &-\sum_i\frac{1}{8\pi^2}\left\{\nu\left[8\mu_i\nu^2-3(2\nu^2+m_i^2)\sqrt{\nu^2+m_i^2}\right]\right.\\ &\left.+3m_i^4\ln\frac{\nu+\sqrt{\nu^2+m_i^2}}{m_i}\right\}-\frac{3\Delta^2\bar{\mu}^2}{\pi^2}+B,\end{aligned} \tag{4}$$

from which one can readily obtain the quark number density for each quark flavor according to the relation $n_i = -\partial\Omega_{\rm CFL}/\partial\mu_i$, i.e.,

$$n_{\rm b} = n_{\rm u} = n_{\rm d} = n_{\rm s} = (\nu^3+2\Delta^2\bar{\mu})/\pi^2, \tag{5}$$

where $n_{\rm b} \equiv (n_{\rm u}+n_{\rm d}+n_{\rm s})/3$ denotes baryon number density.

The energy density is as follows:

$$E = \Omega_{\rm CFL} + \sum_i \mu_i n_i = \Omega_{\rm CFL} + 3n_{\rm b}\bar{\mu} \tag{6}$$

Due to the density-dependent quark mass, the pressure of the system is:

$$P = -\Omega_{\rm CFL} + n_{\rm b}\sum_i \frac{\partial\Omega_{\rm CFL}}{\partial m_i}\frac{{\rm d}m_i}{{\rm d}n_{\rm b}}, \tag{7}$$

where the second term in the right side of the equal sign is crucial to guarantee the thermodynamic consistency, and the derivatives are, respectively, as follows:

$$\frac{\partial\Omega_{\rm CFL}}{\partial m_i} = \frac{3m_i}{2\pi^2}\left[\nu\sqrt{m_i^2+\nu^2} - m_i^2 \times \ln\left(\frac{\nu+\sqrt{m_i^2+\nu^2}}{m_i}\right)\right], \tag{8}$$

and

$$\frac{{\rm d}m_i}{{\rm d}n_{\rm b}} = -\frac{D}{3}n_{\rm b}^{-4/3}. \tag{9}$$

III. GW ECHO FREQUENCY OF CFL SQS IN EQUIVPARTICLE MODEL

To generate the GW echoes, the EOSs of SQM should be sufficiently stiff to feature a photon sphere at $R_{\rm P} = 3GM$. To examine how the stiffness of EOS changes with model parameter D and Δ, we express the velocity of sound as function of $\sqrt{D}$ (upper panel) and Δ (lower panel) with respect to different baryon number densities provided in Fig. 1. Based on the upper panel in Fig. 1, at a fixed $\Delta = 150$ MeV, the velocity of sound decreases as $\sqrt{D}$ increases, indicating a softening of the EOS with larger D. Conversely, with fixed $\sqrt{D} = 100$ MeV, the velocity of sound increases with Δ, which implies that the EOS becomes stiff for large Δ. Therefore, based on Fig. 1, EOS can be inferred to become more stiff by simultaneously reducing D and increasing Δ. Hence, a stiff EOS can be realized by setting $D = 0$ and simultaneously adopting a large Δ. However, the value of Δ cannot be arbitrarily chosen for a given D and is dependent on the density of SQM. To investigate this point, the following steps should be considered.

First, by combing Eqs. (3) and (5) and then eliminating the averaged quark chemical potential $\bar{\mu}$, $\sum_i\sqrt{\nu^2+m_i^2} = \frac{3}{2\Delta^2}(\pi^2 n_{\rm b} - \nu^3)$ can be obtained. Based on this, a function of ν can be introduced, i.e.,

$$\Phi(\nu) = \frac{3}{2\Delta^2}(\pi^2 n_b - \nu^3) - \sum_i\sqrt{\nu^2+m_i^2},\ \ (\nu \geq 0). \tag{10}$$

Here, note that the purpose of introducing the function $\Phi(\nu)$ is only to determine the relation between model parameters D and Δ. Additionally, ν should be considered as a variable of function $\Phi(\nu)$, although it has the meaning of Fermi momentum.

Then, the derivative of $\Phi(\nu)$ can be easily obtained with respect to ν via ${\rm d}\Phi(\nu)/{\rm d}\nu$,

$$\frac{{\rm d}\Phi(\nu)}{{\rm d}\nu} = -\frac{9\nu^2}{2\Delta^2} - \sum_i\frac{\nu}{\sqrt{\nu^2+m_i^2}} \leq 0, \tag{11}$$

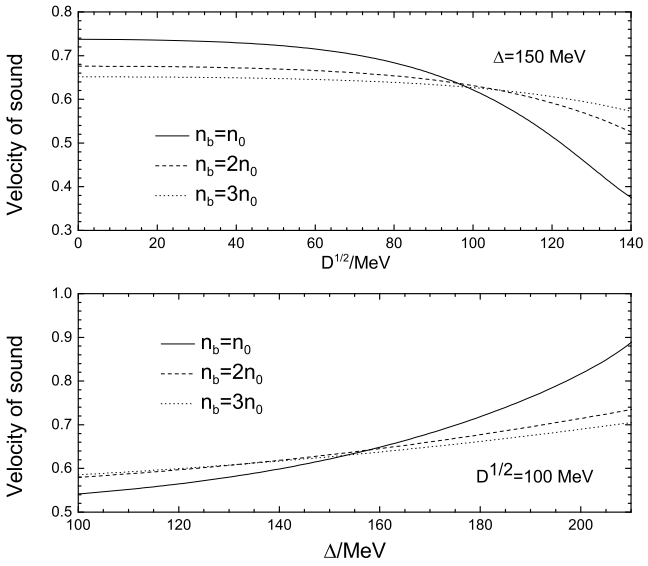

Fig. 1. Velocity of sound as a function of model parameters D (upper panel) and Δ (lower panel) with different given baryon number densities $n_{\rm b}$.

where $\frac{{\rm d}\Phi(\nu)}{{\rm d}\nu}$ is observed to be consistently negative (equal to zero only when $\nu = 0$). This suggests that $\Phi(\nu)$ increases with decreasing ν, and thereby, indicating the existence of a maximum value of $\Phi(\nu)$ at $\nu = 0$, namely

$$\Phi_{\rm max}(\nu = 0) = \frac{3\pi^2 n_{\rm b}}{2\Delta^2} - \sum_i m_i. \tag{12}$$

For Eq. (12), we should indicate that $\nu = 0$ is only a limiting case, and its purpose is to provide the D-Δ window. Additionally, in the following calculations, non-physical values of ν, such as $\nu = 0$, will not be considered.

If Eq. (10) admits a solution for ν, then it implies that the maximum value $\Phi_{\rm max}(\nu = 0)$ should be no less than 0. This in turn yields Eq. (12), i.e., $\Phi_{\rm max}(\nu = 0) \geq 0$, which leads to inequality

$$0 \leq \Delta \leq \pi\sqrt{\frac{3n_{\rm b}}{2\sum_i m_i(n_{\rm b}, D)}}, \tag{13}$$

where the quark mass m_i is explicitly expressed as a function of baryon number density $n_{\rm b}$ and model parameter D.

Evidently, by assigning a value to the model parameter D, the maximum value of Δ can be expressed as a function of baryon number density. Furthermore, the maximum value of Δ increases with n_b for a fixed D. This implies that the highest attainable value of Δ is contingent upon the potential minimal value of the density of SQM for a specific D. Considering that the saturation density of normal nuclear matter is $n_0 \approx 0.16$ fm^{-3}, we assume that the density of SQM is not smaller than n_0, and the minimum baryon number density of SQM is designated to be $n_{\rm b,min}$. To establish a range of values for Δ, we set $n_{\rm b,min} = n_0, 2n_0$, and $3n_0$ in Eq. (13).

In Fig. 2, we present the model parameter window in the $\Delta - D^{1/2}$ diagram for different minimum baryon number den-

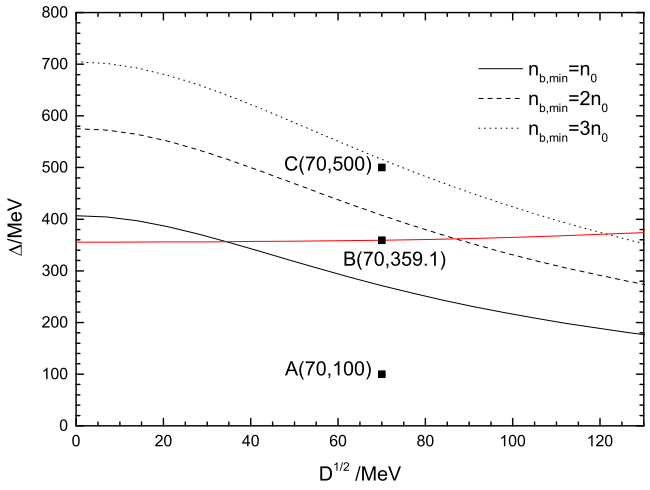

Fig. 2. (Color online) Model parameter window $\Delta - D^{1/2}$ with respect to the given lowest baryon number density $n_{b,\min}$ for SQM. The region bounded by the solid, dashed, and dotted black lines correspond to the solvable EOSs for SQM with the minimum densities that are not less than n_0, $2n_0$, and $3n_0$, respectively. The red line illustrates the correlation between Δ and $D^{1/2}$, which can lead to the most massive SQSs, located precisely on the photon sphere line. The typical model parameters are denoted by solid squares and labeled as A, B, and C.

sities, $n_{\rm b,min}$, of SQM. For instance, if the model parameters lie within the region below the solid black line, a solvable EOS for SQM with a minimum density of $n_{\rm b,min} = n_0$ can be available. The black dashed and dotted lines serve the same purpose but correspond to minimum densities of $2n_0$ and $3n_0$, respectively. Referring to previous study on CFL SQM within this model [39], when assigning a value of $\Delta = 100$ MeV, we find that a solvable EOS spans a broad range of $D^{1/2}$, from 0 to beyond 130 MeV. Notably, as D rises, the maximum value of Δ decreases for a specified $n_{\rm b,min}$. Additionally, increasing $n_{\rm b,min}$ significantly expands the parameter window. For subsequent calculations, we select three representative model parameter sets: $(\sqrt{D}/\mathrm{MeV}, \Delta/\mathrm{MeV}) = (70, 100)$, $(70, 359.1)$, and $(70, 500)$, denoted as sets A, B, and C, respectively, marked by solid squares in Fig. 2.

Before delving into the mass-radius relation for SQSs, we should first check whether condition $\Delta > \frac{m_s^2}{4\bar{\mu}}$ can be fulfilled. This guarantees that the CFL SQM can stably exist [50]. In Fig. 3, we show the difference between Δ and $\frac{m_s^2}{4\bar{\mu}}$ versus baryon number density ranging from n_0 to $10n_0$ for the typical model parameters chosen in FIG. 2. Based on this figure, the difference between Δ and $\frac{m_s^2}{4\bar{\mu}}$ is positive, which implies that the condition $\Delta > \frac{m_s^2}{4\bar{\mu}}$ is fulfilled. Additionally, with increasing baryon number density, the difference becomes significant. Furthermore, the large Δ provides large difference between Δ and $\frac{m_s^2}{4\bar{\mu}}$.

To explore whether the SQSs in the current model can possess a photon sphere and subsequently produce GW echoes, one should first calculate the EOSs for CFL SQM. Following

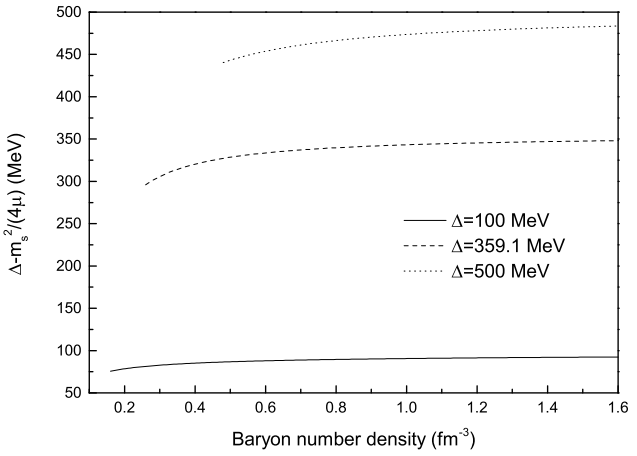

Fig. 3. Difference between Δ and $\frac{m_s^2}{4\bar{\mu}}$ versus baryon number density. The difference is observed to be positive, which implies that the condition $\Delta > \frac{m_s^2}{4\bar{\mu}}$ is fulfilled.

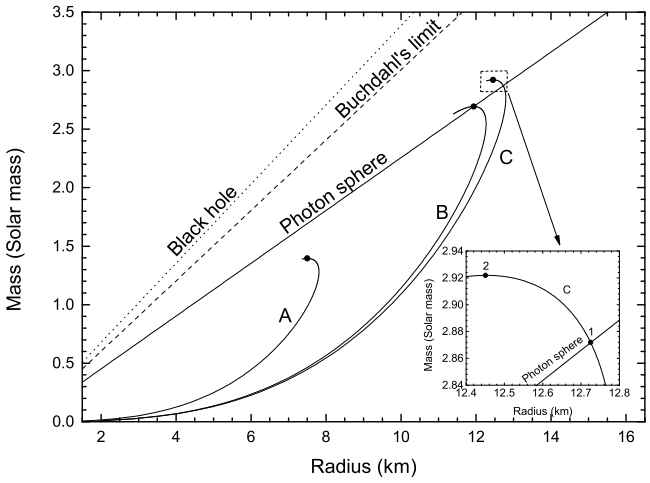

Fig. 4. Mass-radius relation of SQSs in the EOSs within the equivparticle model with typical model parameter sets labeled as A, B, and C. The values of parameter sets are $(\sqrt{D}/\mathrm{MeV}, \Delta/\mathrm{MeV}) = (70, 100)$, $(70, 359.1)$, and $(70, 500)$ for A, B, and C, respectively, as shown in Fig. 2 with solid squares. The maximum masses in these cases are indicated with solid dots.

this, the mass-radius relation for hydrostatically equilibrated SQSs can be determined by solving the TOV equations. The TOV equations are:

$$\frac{\mathrm{d}P}{\mathrm{d}r} = (E+P)\frac{G(m+4\pi r^3 P)}{2Gmr - r^2}, \tag{14}$$

$$\frac{\mathrm{d}m}{\mathrm{d}r} = 4\pi r^2 E, \tag{15}$$

where E and P denote the energy density and pressure at radius r, $G = 6.707 \times 10^{-45}$ MeV^{-2} is the gravitational constant, and $m(r)$ denotes the gravitational mass within the radius r.

The resulting mass-radius relations are illustrated in Fig. 4. Based on this figure, when $\Delta = 100$ MeV, the maximum

mass for case A is determined to be below the photon sphere line. This implies that no GW echoes can be generated in this case. While when $\Delta = 359.1$ MeV, the maximum mass of the SQS nicely locates at the photon sphere line, signifying the critical state for the SQS to possess a photon sphere. For a larger value of $\Delta = 500$ MeV, the EOS corresponding to the maximum mass of SQSs surpasses the photon sphere line, indicating its capability to produce GW echoes. This suggests that the configurations for the SQSs, ranging from point 1 to point 2 in the detailed review profile shown in Fig. 4, exhibit the potential to generate GW echoes. Thus, for a fixed value of $\sqrt{D}$ (specifically, $\sqrt{D} = 70$ MeV in this instance), the maximum mass of SQS, represented by solid dots in Fig. 4, increases with Δ. This correlation is further emphasized in Fig. 1, where the velocity of sound rises concomitantly with Δ. Moreover, for a constant $\sqrt{D}$, a specific Δ value can be determined that positions the maximum mass of the SQS exactly on the photon sphere line.

In Fig. 2, the red line illustrates the correlation between Δ and $D^{1/2}$, which can lead to the most massive SQSs located precisely on the photon sphere line. Furthermore, with an error in the level of 0.1%, it can be fitted as

$$\Delta = \Delta_{\rm min} + \sum_{i=1}^{3} \left(\frac{\sqrt{D}/{\rm MeV}}{c_i} \right)^i \ {\rm MeV}, \qquad (16)$$

where the coefficients are $c_1 \approx 114.5837$, $c_2 \approx 85.3983$, and $c_3 \approx 52.5021$. Based on this equation, parameter Δ is found to increases with $\sqrt{D}$ and Δ, and the first term $\Delta_{\rm min} \approx 355.6398$ MeV is the minimum value of Δ at $D = 0$. This means that the SQM in the CFL state within the current model can satisfy the requirement of featuring a photon sphere for SQS. Consequently, the parameter sets $(\sqrt{D}, \Delta)$ that qualify SQSs to produce GW echoes should lie above the red line illustrated in Fig. 2. Hence, only the parameter set C aligns with the SQS configurations requisite for generating GW echoes. Additionally, from Eqs. (13) and (16), we deduce that the least density necessary for SQM to feature a photon sphere within this model is around $n_{\rm b,min} \approx 0.1223$ fm^{-3}.

To derive the frequency of GW echoes, the time taken for light to traverse from the center of the star to its photon sphere [20] should be computed, i.e.,

$$\tau_{\rm echo} = \int_0^{3GM} \frac{{\rm d}r}{\sqrt{e^{2\Phi(r)}(1 - \frac{2Gm(r)}{r})}}, \qquad (17)$$

When $0 < r < R$, $m(r) = \frac{4\pi}{3} E r^3$. The gravitational potential, $\Phi(r)$, can be derived by integrating the subsequent differential equation, i.e.,

$$\frac{{\rm d}\Phi(r)}{{\rm d}r} = -\frac{1}{E+P}\frac{{\rm d}P}{{\rm d}r}, \qquad (18)$$

which can be solved together with the TOV equations in Eqs. (14) and (15); When $R < r < 3GM$, $m(r) = M$, $e^{2\Phi} = 1 - 2M/r$, and $P = \rho = 0$. Here, P and E denote the pressure and energy density, respectively, as determined by the EOS. Finally, the GW echo frequency can be evaluated by $\omega_{\rm echo} = \pi/\tau_{\rm echo}$.

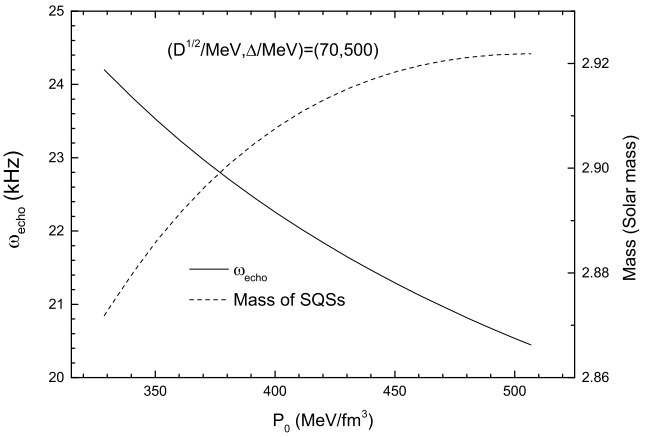

Fig. 5. Frequency of GW echo $\omega_{\rm echo}$ and the mass of SQS as functions of central pressure P_0.

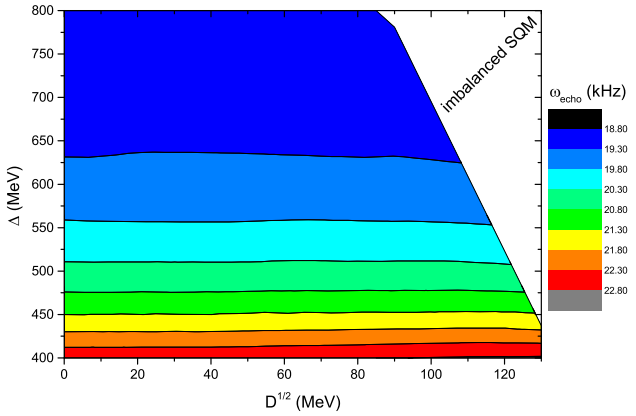

Fig. 6. (Color online) GW echo frequency $\omega_{\rm echo}$ for the most massive SQS in the model parameter window.

In Fig. 5, we present the GW echo frequency $\omega_{\rm echo}$ and the mass of SQS versus central pressure P_0 for case C from point 1 to point 2 in the detailed review profile in Fig. 4. Evidently, as shown in Fig. 5, the mass of SQS increases with central pressure, while the GW echo frequency decreases. In fact, this can be interpreted as follows: with higher pressure, the SQS will have a larger mass. Based on $R_{\rm p} = 3GM$, the photon sphere will be situated further from the center of the SQS. This will result in light requiring more time to travel from the center of the SQS to the photon sphere, thereby leading to a smaller $\omega_{\rm echo}$. Therefore, given the appropriate model parameters, the most massive SQS exhibits the lowest GW echo frequency.

In Fig. 6, we show the GW echo frequencies for the most massive SQSs within the model parameter window where Δ and $\sqrt{D}$ are in the range of 400-800 MeV and 0-130 MeV, respectively. According to Fig. 2, the selected model parameter ranges ensure that the most massive SQSs are positioned above the photon sphere line, thereby capacitating them to

generate GW echoes. Notably, with a constant Δ, a negligible shift is observed in the GW echo frequency as D escalates. Conversely, with a stable D, the GW echo frequency undergoes notable variation with changes in Δ; specifically, it transitions from approximately 22.8 kHz at $\Delta = 400$ MeV to approximately 18.8 kHz at $\Delta = 800$ MeV. In conclusion, the GW echo frequencies predominantly oscillate around 20 kHz in this model, which aligns with the GW frequency magnitudes reported in prior studies [20, 24, 31]. Additionally, the unmarked region designated as imbalanced SQM in the figure signifies scenarios where both Δ and D are substantially elevated, causing the CFL SQM to be unable to maintain pressure equilibrium. This leads to the unstable existence of the SQS.

IV. SUMMARY

In this study, we investigated the GW echoes generated by SQSs within the framework of an equivparticle model. Distinct from prior research that relied on the basic MIT bag model with predetermined sound velocities, our approach utilized EOSs for SQM in the equivparticle model enriched with density-dependent quark masses. This integration not only encapsulates confinement but also quark pairing effects. Significantly, our findings emphasized the crucial role of quark pairing effects to enable a photon sphere and thereby facilitate the production of a GW echo. As the value of Δ increases, the EOS for SQM becomes more stiff, allowing the mass-radius relation of SQS to intersect with the photon sphere line and, therefore, yield GW echoes. Additionally, for specific model parameters Δ and D, the SQS bearing the maximum mass showcases the lowest GW echo frequency. We also estimated the GW echo frequencies for the most massive SQSs within the chosen model parameters. Conclusively, while D imparts minimal influence on the GW echo frequency, an increment in Δ results in significant alterations. The predominant GW echo frequencies hover around 20 kHz, which contrasts with the observed 72 Hz signal in the GW170817 event. This underscores that SQSs, as conceptualized in our current model, should not be construed as ultra-compact objects radiating such low-frequency GW echoes. Future research may need to consider additional effects or avenues [28, 51, 52].

AUTHOR CONTRIBUTIONS

All authors contributed to the study conception and design. Material preparation, data collection and analysis were performed by Jian-Feng Xu, Lei Cui, Zhen-Yan Lu, Cheng-Jun Xia and Guang-Xiong Peng. The first draft of the manuscript was written by Jian-Feng Xu and all authors commented on previous versions of the manuscript. All authors read and approved the final manuscript.

DATA AVAILABILITY STATEMENT

The data that support the findings of this study are openly available in Science Data Bank atttps://www.doi.org/10.57760/sciencedb.12532 andttps://cstr.cn/31253.11.sciencedb.12532.

CONFLICT OF INTEREST

The authors declare that they have no competing interests.

[1] B.P. Abbott, R. Abbott, T.D. Abbott, et al., Observation of gravitational waves from a binary black hole merger. Phys. Rev. Lett. **116**, 061102 (2016). doi:10.1103/PhysRevLett.116.061102

[2] B.P. Abbott, R. Abbott, T.D. Abbott, et al., Gw170817: Observation of gravitational waves from a binary neutron star inspiral. Phys. Rev. Lett. **119**, 161101 (2017). doi:10.1103/PhysRevLett.119.161101

[3] B.P. Abbott, R. Abbott, T.D. Abbott, et al., Gwtc-1: A gravitational-wave transient catalog of compact binary mergers observed by ligo and virgo during the first and second observing runs. Phys. Rev. X **9**, 031040 (2019). doi:10.1103/PhysRevX.9.031040

[4] B.P. Abbott, R. Abbott, T.D. Abbott, et al., All-sky search for continuous gravitational waves from isolated neutron stars using advanced ligo o2 data. Phys. Rev. D **100**, 024004 (2019). doi:10.1103/PhysRevD.100.024004

[5] R. Abbott, et al., GW190814: Gravitational Waves from the Coalescence of a 23 Solar Mass Black Hole with a 2.6 Solar Mass Compact Object. Astrophys. J. Lett. **896**, L44 (2020). doi:10.3847/2041-8213/ab960f

[6] B.P. Abbott, R. Abbott, T.D. Abbott, et al., Multi-messenger observations of a binary neutron star merger. The Astrophysical Journal **848**, L12 (2017). doi:10.3847/2041-8213/aa91c9

[7] B.P. Abbott, R. Abbott, T.D. Abbott, et al., Gw170817: Measurements of neutron star radii and equation of state. Phys. Rev. Lett. **121**, 161101 (2018). doi:10.1103/PhysRevLett.121.161101

[8] V. Cardoso, E. Franzin, P. Pani, Is the gravitational-wave ringdown a probe of the event horizon? Phys. Rev. Lett. **116**, 171101 (2016). [Erratum: Phys.Rev.Lett. 117, 089902 (2016)]. doi:10.1103/PhysRevLett.116.171101

[9] V. Cardoso, S. Hopper, C.F.B. Macedo, et al., Gravitational-wave signatures of exotic compact objects and of quantum corrections at the horizon scale. Phys. Rev. D **94**, 084031 (2016). doi:10.1103/PhysRevD.94.084031

[10] G. D'Amico, N. Kaloper, Black hole echoes. Phys. Rev. D **102**, 044001 (2020). doi:10.1103/PhysRevD.102.044001

[11] R.S. Conklin, B. Holdom, J. Ren, Gravitational wave echoes through new windows. Phys. Rev. D **98**, 044021 (2018). doi:10.1103/PhysRevD.98.044021

[12] G. Ashton, O. Birnholtz, M. Cabero, et al., Comments on: "Echoes from the abyss: Evidence for Planck-scale structure at black hole horizons". arXiv:1612.05625 [gr-qc] . arXiv:1612.05625

[13] J. Abedi, H. Dykaar, N. Afshordi, Echoes from the Abyss: The Holiday Edition! arXiv:1701.03485 [gr-qc] . arXiv:1701.03485

[14] J. Westerweck, A.B. Nielsen, O. Fischer-Birnholtz, et al., Low significance of evidence for black hole echoes in gravitational wave data. Phys. Rev. D **97**, 124037 (2018). doi:10.1103/PhysRevD.97.124037

[15] J. Abedi, H. Dykaar, N. Afshordi, Comment on: "Low significance of evidence for black hole echoes in gravitational wave data". arXiv:1803.08565 .

[16] H. Nakano, N. Sago, H. Tagoshi, et al., Black hole ringdown echoes and howls. PTEP **2017**, 071E01 (2017). arXiv:1704.07175, doi:10.1093/ptep/ptx093

[17] Z. Mark, A. Zimmerman, S.M. Du, et al., A recipe for echoes from exotic compact objects. Phys. Rev. D **96**, 084002 (2017). doi:10.1103/PhysRevD.96.084002

[18] C. Barceló, R. Carballo-Rubio, L.J. Garay, Gravitational wave echoes from macroscopic quantum gravity effects. JHEP **05**, 054 (2017). doi:10.1007/JHEP05(2017)054

[19] J. Abedi, N. Afshordi, Echoes from the Abyss: A highly spinning black hole remnant for the binary neutron star merger GW170817. JCAP **11**, 010 (2019). doi:10.1088/1475-7516/2019/11/010

[20] P. Pani, V. Ferrari, On gravitational-wave echoes from neutron-star binary coalescences. Class. Quant. Grav. **35**, 15LT01 (2018). doi:10.1088/1361-6382/aacb8f

[21] S. Xin, B. Chen, R.K.L. Lo, et al., Gravitational-wave echoes from spinning exotic compact objects: Numerical waveforms from the teukolsky equation. Phys. Rev. D **104**, 104005 (2021). doi:10.1103/PhysRevD.104.104005

[22] A. Urbano, H. Veermäe, On gravitational echoes from ultracompact exotic stars. Journal of Cosmology and Astroparticle Physics **2019**, 011 (2019). doi:10.1088/1475-7516/2019/04/011

[23] H.A. Buchdahl, General relativistic fluid spheres. Phys. Rev. **116**, 1027–1034 (1959). doi:10.1103/PhysRev.116.1027

[24] M. Mannarelli, F. Tonelli, Gravitational wave echoes from strange stars. Phys. Rev. D **97**, 123010 (2018). doi:10.1103/PhysRevD.97.123010

[25] E. Witten, Cosmic separation of phases. Phys. Rev. D **30**, 272–285 (1984). doi:10.1103/PhysRevD.30.272

[26] E. Farhi, R.L. Jaffe, Strange matter. Phys. Rev. D **30**, 2379–2390 (1984).

[27] F. Weber, Strange quark matter and compact stars. Progress in Particle and Nuclear Physics **54**, 193 – 288 (2005). doi:https://doi.org/10.1016/j.ppnp.2004.07.001

[28] R.X. Xu, Can cold quark matter be solid? Int. J. Mod. Phys. D **19**, 1437–1446 (2010).

[29] D. Kartini, A. Sulaksono, Gravitational wave echoes from quark stars. J. Phys. Conf. Ser. **1572**, 012034 (2020). doi:10.1088/1742-6596/1572/1/012034

[30] P.C. Chu, Y. Zhou, X. Qi, et al., Isospin properties in quark matter and quark stars within isospin-dependent quark mass models. Phys. Rev. C **99**, 035802 (2019). doi:10.1103/PhysRevC.99.035802

[31] C. Zhang, Gravitational wave echoes from interacting quark stars. Phys. Rev. D **104**, 083032 (2021). doi:10.1103/PhysRevD.104.083032

[32] J. Bora, D.J. Gogoi, U.D. Goswami, Strange stars in f(R) gravity palatini formalism and gravitational wave echoes from them. JCAP **09**, 057 (2022). doi:10.1088/1475-7516/2022/09/057

[33] J. Bora, U.D. Goswami, Gravitational wave echoes from compact stars in f(R,T) gravity. Phys. Dark Univ. **38**, 101132 (2022). doi:10.1016/j.dark.2022.101132

[34] J. Bora, U. Dev Goswami, Gravitational Wave Echoes from Strange Stars for Various Equations of State. Springer Proc. Phys. **277**, 673–677 (2022). doi:10.1007/978-981-19-2354-8$_1$22

[35] C. Zhang, Y. Gao, C.J. Xia, et al., Rescaling strangeon stars and its implications on gravitational-wave echoes. arXiv:2305.13323 .

[36] G. Fowler, S. Raha, R. Weiner, Confinement and Phase Transitions. Z. Phys. C 26 (1981). doi:10.1007/BF01410668

[37] G.X. Peng, H.C. Chiang, J.J. Yang, et al., Mass formulas and thermodynamic treatment in the mass-density-dependent model of strange quark matter. Phys. Rev. C **61**, 015201 (1999). doi:10.1103/PhysRevC.61.015201

[38] G.X. Peng, H.C. Chiang, B.S. Zou, et al., Thermodynamics, strange quark matter, and strange stars. Phys. Rev. C **62**, 025801 (2000).

[39] Y.D. Chen, , G.X. Peng, et al., Color-flavor locked strange quark matter in a mass density-dependent model. High Energy Physics and Nuclear Physics **31**, 3 (2007).

[40] S.W. Chen, L. Gao, G.X. Peng, One-gluon-exchange effect on the properties of quark matter and strange stars. Chin. Phys. C **36**, 947–953 (2012). doi:10.1088/1674-1137/36/10/005

[41] C.J. Xia, G.X. Peng, S.W. Chen, et al., Thermodynamic consistency, quark mass scaling, and properties of strange matter. Phys. Rev. D **89**, 105027 (2014). doi:10.1103/PhysRevD.89.105027

[42] G.X. Peng, S.W. Chen, Q. Chang, et al., Quark confinement and the properties of quark matter. Int. J. Mod. Phys. E **19**, 1837 (2010). doi:10.1142/S0218301310016272

[43] P.C. Chu, L.W. Chen, QUARK MATTER SYMMETRY ENERGY AND QUARK STARS. Astrophys. J. **780**, 135 (2014). doi:10.1088/0004-637x/780/2/135

[44] L. Wang, J. Hu, C.J. Xia, et al., Stable up-down quark matter nuggets, quark star crusts, and a new family of white dwarfs. Galaxies **9**, 70 (2021). doi:10.3390/galaxies9040070

[45] J.F. Xu, D.B. Kang, G.X. Peng, et al., Bulk viscosity for interacting strange quark matter and r-mode instability windows for strange stars. Chin. Phys. C **45**, 015103 (2021). doi:doi:10.1088/1674-1137/abc0cd

[46] J.F. Xu, Bulk viscosity of interacting magnetized strange quark matter. Nucl. Sci. Tech. **32**, 111 (2021). doi:10.1007/s41365-021-00954-3

[47] J.F. Xu, C.J. Xia, Z.Y. Lu, et al., Symmetry energy of strange quark matter and tidal deformability of strange quark stars. Nucl. Sci. Tech. **33**, 143 (2022). doi:10.1007/s41365-022-01130-x

[48] E. Fonseca, et al., The NANOGrav Nine-year Data Set: Mass and Geometric Measurements of Binary Millisecond Pulsars. Astrophys. J. **832**, 167 (2016).

[49] K.A. Olive, et al., Review of Particle Physics. Chin. Phys. C **38**, 090001 (2014). doi:10.1088/1674-1137/38/9/090001

[50] M. Alford, K. Rajagopal, Absence of two flavor color superconductivity in compact stars. JHEP **06**, 031 (2002).

[51] X. Lai, R. Xu, Strangeon and Strangeon Star. J. Phys. Conf. Ser. **861**, 012027 (2017). doi:10.1088/1742-6596/861/1/012027

[52] J. Lu, R. Xu, Strangeon Stars. JPS Conf. Proc. **20**, 011026 (2018). doi:10.7566/JPSCP.20.011026